Journal of Wind Engineering & Industrial Aerodynamics 251 (2024) 105805

Contents lists available at ScienceDirect

Journal of Wind Engineering & Industrial Aerodynamics

journal homepage: www.elsevier.com/locate/jweia

The influence of thunderstorm type on extreme near-surface wind speeds: Iowa case study

David T. Roegner [a,*], Franklin T. Lombardo [a], Zachary B. Wienhoff [b], Daniel M. Rhee [c], Melissa A. Wagner [d,e], Richard L. Wood [f]

[a] University of Illinois Urbana-Champaign, Urbana, 61801, IL, USA
[b] Haag Engineering Company, Flour Mound, 75028, TX, USA
[c] National Institute of Standards and Technology, 20899, Gaithersburg, MD, USA
[d] Cooperative Institute for Severe and High Impact Weather Research and Operations, 73072, Norman, OK, USA
[e] National Severe Storm Laboratory, 73072, Norman, OK, USA
[f] University of Nebraska-Lincoln, 68588, Lincoln, NE, USA

ABSTRACT

The derecho of August 10, 2020 that impacted Iowa and neighboring states is the costliest thunderstorm disaster in U.S. history. A derecho, which features prolonged and destructive winds, is a type of thunderstorm which has different near-surface wind generating mechanisms than typically assumed in wind engineering. The derecho event prompted two research questions with respect to wind engineering: (1) should derechos, and more broadly thunderstorm type, be considered separately? and (2) how unique is this particular derecho event?

Wind speeds for design in the U.S. are currently estimated using an approach where probability distributions of all thunderstorm winds are analyzed through a mixed distribution. Using Automated Surface Observing System (ASOS) and radar data from the National Weather Service, thunderstorm events with ASOS wind speeds >58 mph (26 m/s) were classified by thunderstorm type: single-cell, multicellular, or supercell thunderstorms in Iowa. An extreme value analysis was done on each thunderstorm type. Multicellular thunderstorms, like the August 2020 derecho, dominate the extreme wind climatology in Iowa. Evaluating the uniqueness of the derecho event required a post-damage assessment. Analysis from failed and unfailed street signs and nearby anemometry was used to estimate peak wind speeds approaching 120 mph (50 m/s).

1. Overview

Thunderstorm winds are responsible for a significant amount of loss every year in the United States and dominate the extreme wind climate across much of the world (Doswell et al., 2005; Kelly et al., 1985; Lombardo and Zickar, 2019). One such event was the August 10, 2020, derecho that affected Iowa and surrounding states. This event caused $11B in insured losses (NOAA, 2020a), with a significant proportion of these losses as a result of crop damage, making it the costliest thunderstorm event in U.S. history.

Current design wind loads are calculated, in part, using an extreme-value analysis of thunderstorm wind speed data collected from ASOS stations (National Weather Service, 1998). In wind engineering, storm type has generally been a binary classification procedure. These classifications are thunderstorm and non-thunderstorm and/or synoptic and non-synoptic (e.g., Lombardo et al., 2009; Solari, 2014; Vallis et al., 2019). Design wind maps include both synoptic and non-synoptic winds in a mixed probability distribution. ASOS data also includes ‘flags’ for thunderstorms occurring at or near the site which are then used to classify wind speeds as belonging to thunderstorms (e.g., Lombardo, 2012). However, extreme surface wind production within thunderstorms varies depending on the thunderstorm type, and thunderstorm types have shown different physical and probabilistic characteristics. For example, Lombardo et al. (2014) showed different timescales and profile behavior for different thunderstorm types where events with shorter time scales showed a more uniform or impinging jet (nose) profile while the longer duration event (i.e., mesoscale convective system or MCS) had a logarithmic profile. Similarly, Lombardo and Zickar (2020) showed that microburst events (i.e., isolated downbursts) have a sharper peak and shorter time duration as compared to an MCS. These differences will likely cause a variation in spatial and temporal characteristics in thunderstorm winds at the surface and may influence wind loading.

In meteorology, thunderstorm types are generally classified into single-cell thunderstorms, multicellular thunderstorms, and supercell thunderstorms (e.g., Weisman and Klemp, 1982; Markowski and

---

[*] Corresponding author.
E-mail address: dtr2@illinois.edu (D.T. Roegner).

https://doi.org/10.1016/j.jweia.2024.105805
Received 9 November 2023; Received in revised form 18 June 2024; Accepted 18 June 2024

Richardson, 2010; Trapp, 2013). The thunderstorm type can be distinguished through the examination of thunderstorm characteristics using remote sensing tools like Doppler radar, and via assessment of environmental parameters such as wind shear and instability (Weisman and Klemp, 1982). Wind shear is the change in wind speed or direction with height. Instability can be estimated using the parameter of convective available potential energy, or CAPE. Notably, the product of the 0–6 km shear and CAPE (Significant Severe Parameter) has been shown to detect potential severe storm environments where hail greater than 2 inches (5 cm) in diameter, wind greater than 75 mph (33.5 m/s) or a tornado of F2 strength or greater is more likely to occur (Brooks et al., 2003). However, this does not differentiate between the thunderstorm types causing these hazards. Weisman and Klemp (1982) found that both shear and instability were important to thunderstorm morphology between single-cell thunderstorms, multicellular thunderstorms, and supercell thunderstorms. However, as noted in Markowski and Richardson (2010), it is common to use only the shear value when determining thunderstorm type since thunderstorm type is a stronger function of vertical wind shear than CAPE. Single-cell thunderstorms are typically associated with shear values less than 10 m/s; multicellular thunderstorms are favorable in highly buoyant environments with shear values between 5 and 15 m/s; and lastly supercell thunderstorms are favorable in environments with shear greater than 20 m/s. It is important to note that not every case follows the theory outlined by Weisman and Klemp (1982).

In addition to the assessment of environmental variables, Doppler radar can be used. The use of Doppler radar to identify each thunderstorm type is discussed in a future section. The Doppler radar parameters that are most important to understand are reflectivity and velocity. Radar reflectivity represents the amount of energy that is returned to the radar where higher values represent more intense rainfall and larger drops (Marshall et al., 1947; Wexler and Swingle, 1947). Radial velocity plots show the average speed at which the targets are moving towards or away from the radar. While not the focus of this specific study, near surface wind speed estimates utilizing radial velocity data can be done in events within 6 miles (10 km) of a radar (Ibrahim et al., 2023). For this study, the radial velocity and reflectivity data is used to differentiate between thunderstorm types. The process in categorizing these thunderstorm events from low-level Doppler radar data and the importance of understanding the dynamics of the different thunderstorm types and associated surface wind production mechanisms for wind engineering is discussed in subsequent sections.

1.1. *Thunderstorm types*

Single-cell thunderstorms are typically short lived (Table 1) and often isolated. Fig. 1 depicts a single cell thunderstorm and the evolution of this thunderstorm type. The beginning stage of a single-cell thunderstorm is the rising of air that is more buoyant than the surrounding environment. The water vapor in the rising air eventually condenses allowing us to see the cloud. This beginning stage is shown in Fig. 1a. Fig. 1b shows that the single-cell thunderstorm continues to grow in height, and large hydrometeors begin to form. Once the hydrometeors become too heavy, the updraft can no longer support them, and they fall back through the updraft due to the weak wind shear (Doswell, 1985). As these hydrometeors fall through the updraft, the air cools. This cooling will make the air less buoyant inside the cloud, thus weakening the updraft and allowing for the hydrometeors and air to descend towards the ground as seen in Fig. 1c. Due to the weakening of the updraft, the lifespan of a single-cell thunderstorm is on the order of 1 h (Byers and Braham, 1948; Doswell, 1985). Wind gusts in single-cell thunderstorms are due to the descending air in the downdraft (Wakimoto, 2001). This descending air eventually reaches the ground, and once at the ground, the only direction the air can move is outward. If the descending air has significant momentum, the resulting outflow is termed a ‘downburst’ and is conceptually how wind engineering has viewed all thunderstorm generated winds (Gunter and Schroeder, 2015). However, other thunderstorm types produce extreme near surface winds in different ways, and understanding how these storms form and produce these winds are essential for the wind engineering community to understand in order to make advancements in wind load design for non-synoptic wind events.

Table 1
The spatial, temporal and mechanisms responsible for the surface-based winds in the three thunderstorm types discussed. The time and spatial scales are approximated, and it is possible to have thunderstorms of a category that do not fit within the scales described.

Thunderstorm Type	Time Scale	Spatial Scale	Wind Production Mechanisms
Single-Cell	<1 h	<50 km	Evaporative cooling and hydrometeor loading
Multicellular	>1 h	>50 km	Rear inflow jet, mesovortices, evaporative cooling
Supercell	>1 h	<50 km	FFD, RFD, evaporative cooling

For multicellular thunderstorms, the spatial and temporal scales are larger (see Table 1). Multicellular thunderstorms consist of multiple single-cell thunderstorms at various stages of maturity. This will cause the multicellular thunderstorms to go through cycles that result in multiple updrafts, or cells, to develop. As the outflow of the thunderstorm spreads, the system will grow in scale. Eventually, these thunderstorms can become organized in a linear fashion and are categorized as an MCS. An example of an MCS and the individual cells at different life stages is depicted in Fig. 2a. An MCS is defined as an axis of intense precipitation spanning at least 100 km (62 mi) and comprising of an area of weaker stratiform precipitation (Houze, 1993). Examples of these organized MCS thunderstorms are derechos, bow echoes, and squall lines (NOAA National Severe Storms Laboratory, n.d.). Like single-cell thunderstorms, the source of straight-line winds can be caused by a downdraft, but it can also be caused by the *rear inflow jet* (Weisman, 1992) or *mesovortices* (Trapp and Weisman, 2003). The rear inflow jet is formed when a horizontal buoyancy gradient or pressure gradient occurs in the thunderstorm. This is evident in Fig. 2a where the “L” in the center of the MCS represents an area of lower pressure. This will cause the gradient which draws environmental air from behind the storm into the thunderstorm. This air descends and may eventually reach the ground, propagating outward and creating straight line winds as seen by the arrow labeled “descending rear inflow” in Fig. 2a. These winds associated with the rear inflow jet originate in the mid-levels, where the background flow is already strong, and the buoyancy gradient amplifies these winds, which can cause significant damage once they reach the surface. Another wind producing process is associated with mesovortices in an MCS (Trapp and Weisman, 2003). It is theorized that these mesovortices cause an area of low-pressure near the surface. Fig. 2b depicts the area of low pressure formed by rotating air as a red blob along the gust front (green line). The downward arrow above the red blob is representative of the downward momentum of the air formed due to a vertical pressure gradient force. This causes air to descend to nearby regions as marked by the gray area on the surface of Fig. 2b. Additionally, this mesovortex induced wind can be additive with the wind caused by the rear inflow jet. A mesovortex can have a diameter between 1 and 12 miles (2 and 20 km) which makes them a small-scale feature, thus extreme winds from mesovortices are thought to impact a small area. Mesovortices may have been first documented by Fujita and Wakimoto (1981), but they were described as downbursts at the time (Schenkman and Xue, 2016). As technology advanced and Doppler radar data and modeling became available, it was discovered that these were most likely not downburst events, rather they were wind events caused by the mesovortex itself. For an overview of mesovortex studies, refer to Schenkman and Xue (2016). Much of the current work with mesovortices includes the genesis and predictability of mesovortices in MCS thunderstorms and the tornadoes they produce (NOAA, 2022).

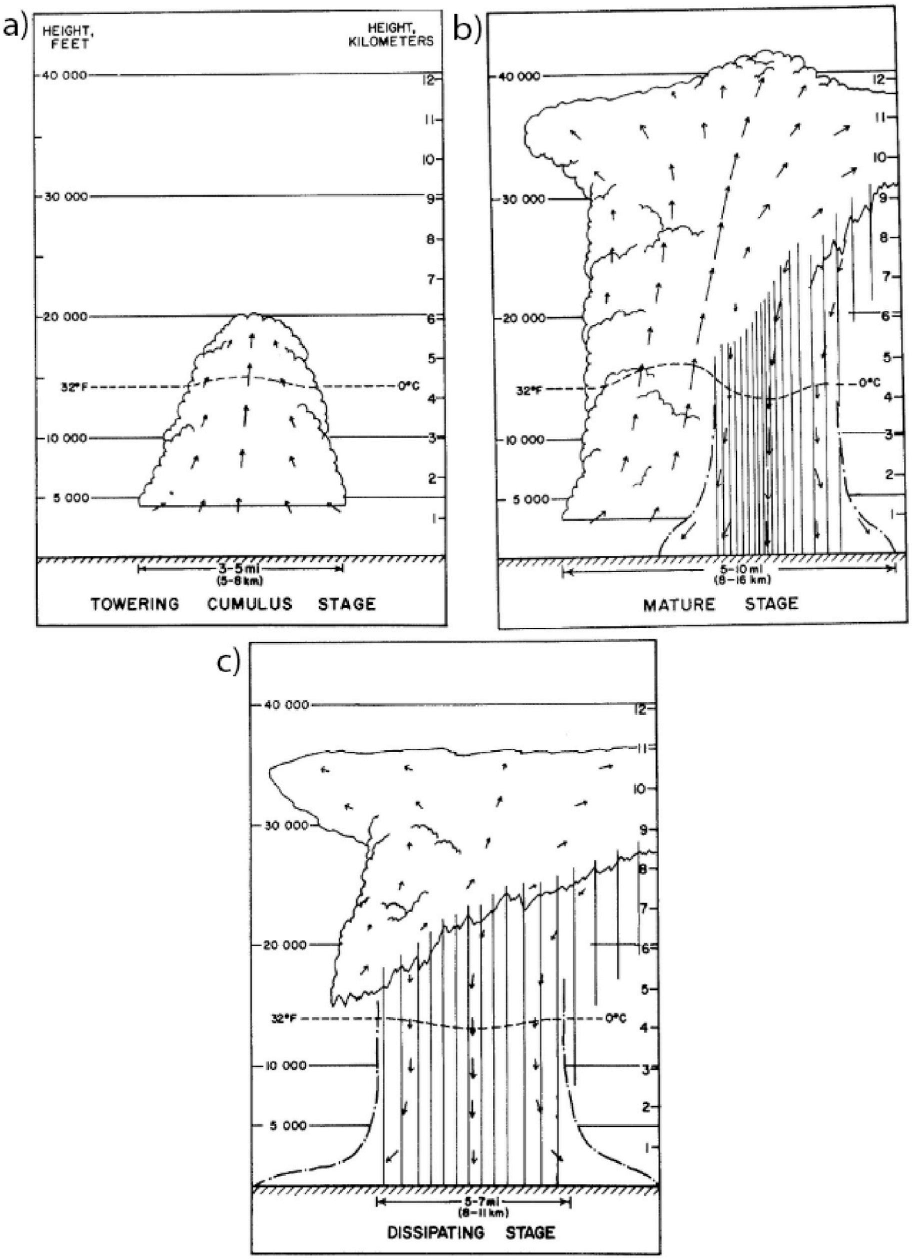

Fig. 1. Schematic showing the lifecycle of a single-cell thunderstorm from Byers and Braham (1948) and modified by Doswell (1985). © American Meteorological Society. Used with permission.

A mesoscale convective system can be defined as a derecho when an area of concentrated wind reports of 58 mph (26 m/s) or more occurs; thunderstorm wind reports cover a major axis length of more than 400 km (250 mi); reports must be continuous; and at least 3 of the reports must be for winds greater than 75 mph (33.5 m/s) (Johns and Hirt, 1987). Many of the wind reports in a derecho are due to both the rear inflow jet and mesovortices (Trapp and Weisman, 2003; Atkins et al., 2005; Wakimoto et al., 2006).

The third thunderstorm type is a supercell. Like a single-cell thunderstorm, a supercell thunderstorm has a small spatial scale on the order of 10 km (6.2 mi) (Table 1). However, supercell thunderstorms can be long lived, due to strong shear (Weisman and Klemp, 1982). A distinct characteristic of a supercell thunderstorm is a rotating updraft evident by the red arrow in Fig. 3. This rotating updraft can help to produce a tornado and is also the location of a hook-like feature on radar data. Two types of downdrafts known as the rear-flank and forward-flank downdraft (RFD and FFD) occur in supercell thunderstorms (Lemon and Doswell, 1979) and are represented in Fig. 3 by the blue arrows. In the forward-flank, hydrometeors falling to the ground evaporate and cool causing a burst of outflow at the ground. The rear-flank downdraft is caused by a pressure gradient between the surface and mid-level of the supercell thunderstorm and the evaporative cooling of hydrometeors (Klemp and Rotunno, 1983; Carbone, 1983). It is a similar process as to mesovortices in MCSs where the rotating air near the ground and in the rotating updraft of the supercell thunderstorm creates a low-pressure area which draws the air inward and downward. If the rotation is intense and near the ground, air can be drawn horizontally inward and vertically downward towards the center of the rotation, when this occurs, it is known as an occlusion downdraft (Davies-Jones, 2006).

1.2. August 10, 2020 derecho

On August 10, 2020, a derecho tracked across Iowa (Fig. 4) with peak wind speed estimates greater than 120 mph (54 m/s) near Cedar Rapids,

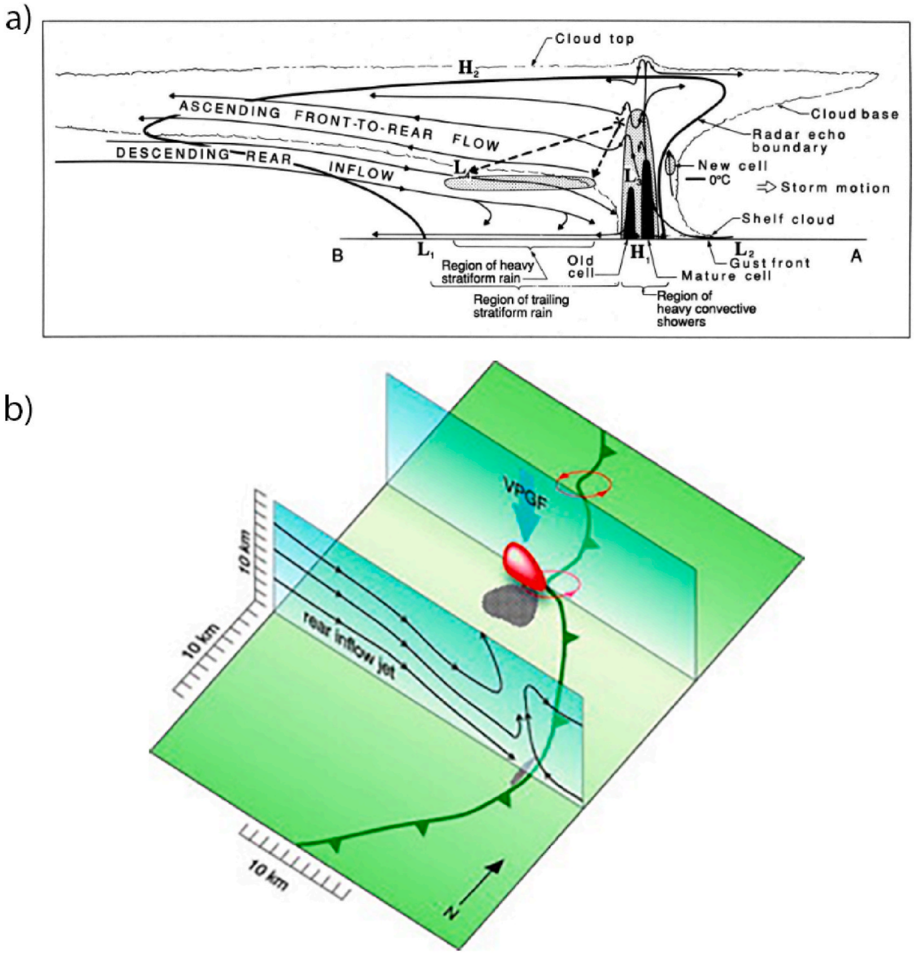

Fig. 2. (a) Plan view model from Houze et al. (1989) depicting the vertical structure of an MCS. (b) a schematic showing how mesovortices may produce surface winds from Trapp and Weisman (2003). © American Meteorological Society. Used with permission.

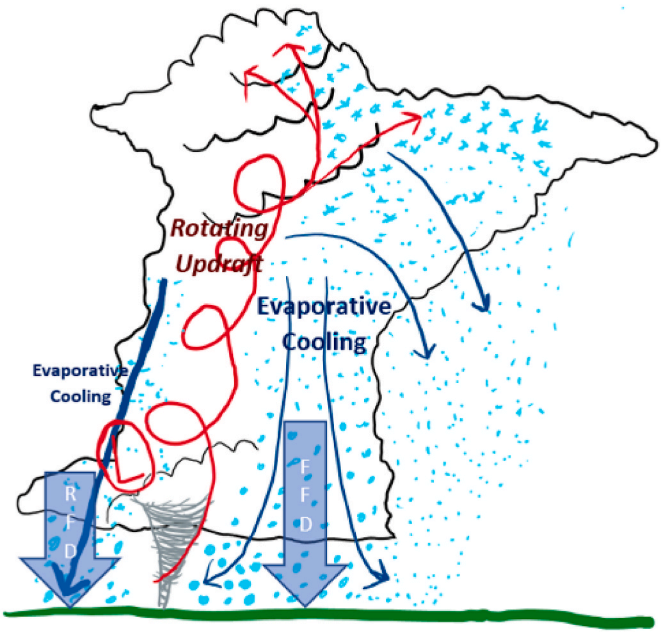

Fig. 3. Schematic showing the components of a supercell and the wind producing mechanisms.

Iowa (NOAA, 2020b). This event is currently the costliest thunderstorm event in U.S. history (NPR, 2020), causing an estimated $11B in insured losses (NOAA, 2020a), with a significant proportion of these losses as a result of crop damage (e.g., corn and soybeans). Based on local accounts and limited field data, this event was unique in that extreme winds capable of causing significant damage persisted for a relatively long period of time, different than what has been assumed due to a 'downburst'. This event was the motivation of this study and prompted the asking of two research questions: (1) should derechos, and their broader thunderstorm type, multicellular thunderstorms, be considered separately when predicting extreme wind speeds for wind load design? and (2) how unique is this particular event in the context of wind engineering?

To answer these questions and given the region's susceptibility to MCS events (Haberlie and Ashley, 2019), this case study focused on two parts. The first was a classification and analysis of thunderstorm types for extreme thunderstorm wind speeds recorded at all ASOS stations in Iowa over about 25 years. Thunderstorm classification was assessed using Doppler radar imagery and once classified, an extreme value analysis was performed. This extreme value analysis used a similar process to the current process used for wind loading in ASCE (American Society of Civil Engineers, 2022) and is discussed in Section 2.

The second focus was a wind speed estimation for the Cedar Rapids area based on a post-thunderstorm assessment done by the authors following the August 10, 2020 event. This estimation included the use of information from other nearby anemometers (non-ASOS) and damage to the built and natural environment. The survey was conducted as the ASOS station in Iowa (Cedar Rapids) lost power near the time of the

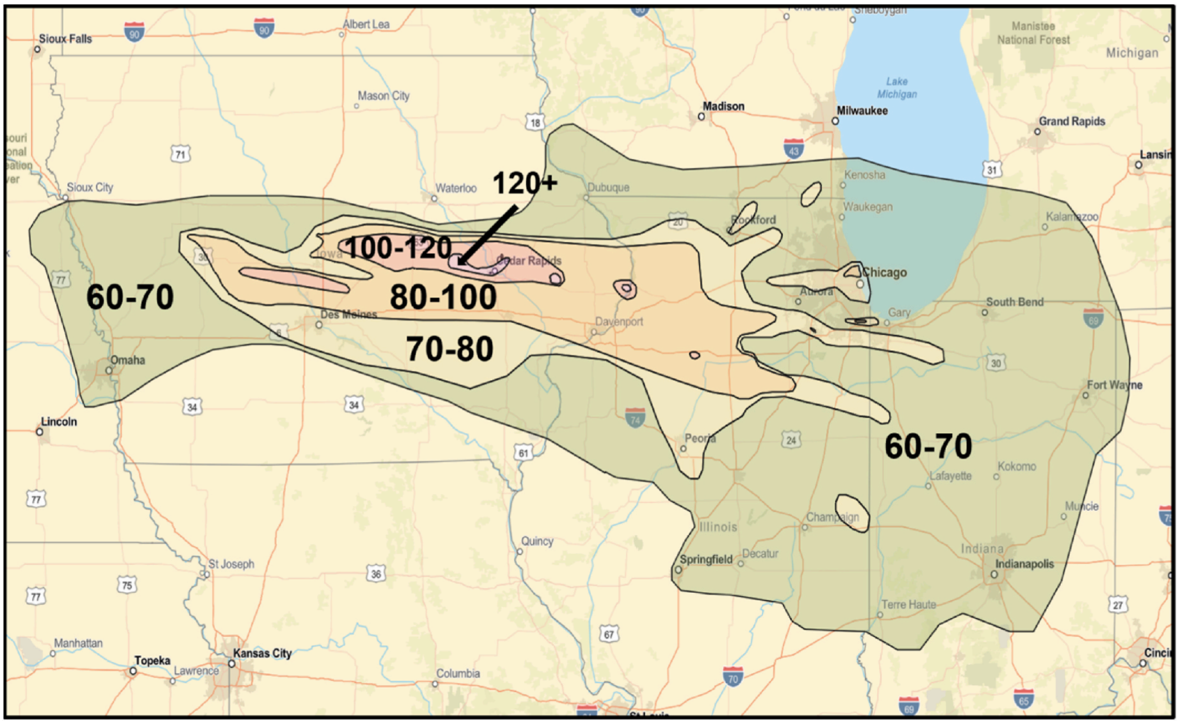

Fig. 4. Swath of the derecho. Estimated wind speeds are in mph courtesy of the NWS. Severe winds occurred across Iowa, Illinois, Indiana and parts of Michigan and Wisconsin.

highest winds, which limited the ability to fully link the damages to wind speed and essentially "losing" the wind speed for extreme value analysis.

2. Thunderstorm classification

2.1. Data

The ASOS stations in Iowa consist of 15 locations. Records on peak wind speeds date back to 1973. In addition to the 15 ASOS stations, Iowa is covered by 6 WSR-88D radars which are operated by the National Weather Service (Fig. 5). Doppler Radar data began in 1995, although there were no significant events in 1995, thus the period selected for analysis is from 1996 to 2022. In 2001, Doppler radar data were not available or not sufficient for 8 of the 10 events, so the year was omitted from the analysis. Doppler radar data were accessed through Next Generation Weather Radar (NEXRAD) on Amazon Web Services (AWS) and is available for free use (https://registry.opendata.aws/noaa-nexrad).

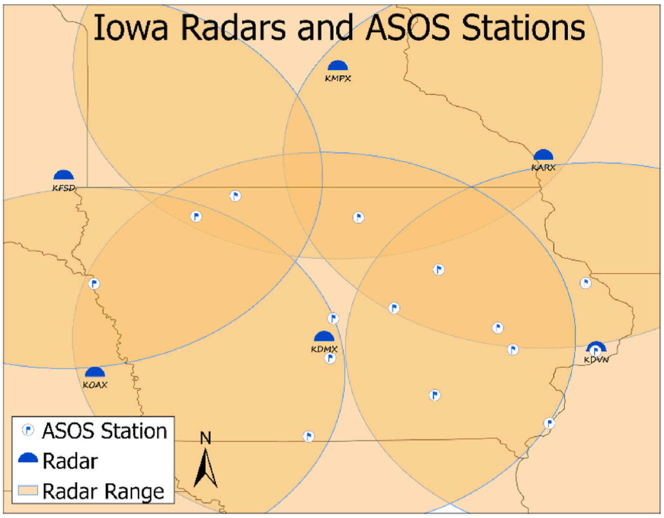

Fig. 5. This map shows the 15 ASOS stations in Iowa and the 6 WSR-88D radars that provide coverage for the state. The range circles are at a radius of 150 miles (241 km) which is the typical range in which radar data is of sufficient quality for analysis.

Initially, a database was created for any thunderstorm event with a wind gust ≥25 kt (29 mph or 13 m/s) based on Lombardo et al. (2009). The database included date, time, thunderstorm event flag, raw (or recorded) wind speed in knots, and standardized 3-s wind speed corrected to 10-m height in mph. The database was then filtered to focus on only the most extreme events, so events with a peak raw wind speed of 50 kt (58 mph or 26 m/s) or more were considered. The criteria of 50 kt was selected as it is the severe criteria of the National Weather Service (National Oceanic and Atmospheric Administration, n.d.). Peak wind speeds from independent thunderstorms were used using the method discussed in Lombardo et al. (2009) and Lombardo (2012).

2.2. Methods

To classify the wind speed data from ASOS into thunderstorm type, a method was developed to extract the date and time of the thunderstorm event from ASOS data and access the Doppler radar data through AWS's database to make a Graphics Interchange Format file (GIF) of the event that showed the reflectivity and velocity plots starting 30 min prior to the gust time to 30 min after the gust time at the lowest elevation scan. The closest radar to the ASOS station was used and the plots had a 3° by 3° domain centered on the ASOS station. The Doppler radar data were then used to manually classify the thunderstorms by thunderstorm type.

In some cases, the single radar station was not able to capture the full extent of the thunderstorm being classified, due to the distance the thunderstorm was to the nearest radar site. In these cases, reflectivity mosaics with a 186 mile by 186 mile (300 km by 300 km) domain were used. These mosaic plots utilize multiple radars rather than a single radar to give a better picture of the spatial extent of the thunderstorm which can be seen in Fig. 6 depicting the August 2020 derecho.

Most cases were easily classified with the single station Doppler radar data by looking at key factors such as spatial coverage and the wind characteristics discerned from the radial velocity plots. When looking at the spatial coverage of the plots, if there was a line of high reflectivity values (>40 dBZ) with an area of lower reflectivity values nearby, fitting the criteria of a mesoscale convective system (Houze, 1993), a multicellular thunderstorm was the likely thunderstorm type. The August 2020 derecho shown in Fig. 6 is a multicellular thunderstorm due to the linear extent of the convective precipitation which is followed by stratiform precipitation to the west. Some multicellular thunderstorm cases may not have fit the mesoscale convective system criteria, so in these cases, the spatial scale of the reflectivity was the main identifying feature where multiple areas of intense precipitation in close proximity indicated the multicellular thunderstorm type.

In areas where there was a large spatial gap between cells, or only one cell was present, a classification between supercell thunderstorm and single-cell thunderstorm was needed. When determining if the thunderstorm mode was a supercell or single-cell, a number of criteria were used. The first criteria would be the total time period the cell appeared on Doppler radar plots. If it was an hour or less, this was a good indication of a single-cell thunderstorm (Byers and Braham, 1948; Doswell, 1985). The velocity plots were then used to confirm the thunderstorm type as single-cell or supercell. The key was looking to see if rotation was present. Rotation was indicated when the color red, winds away from the radar, is right next to the color green, winds towards the radar, forming a small couplet-like feature spanning between 3 miles and 6 miles (5 and 10 km) in diameter (Lemon and Doswell, 1979). This couplet was indicative of the rotating updraft known as a mesocyclone (Burgess, 1976). This methodology was used in addition to the reflectivity plots where a hook-like feature may have also appeared in the area of rotation (Stout and Huff, 1953). Another aspect that indicated a supercell, is the cell splitting into two and moving in opposite directions (Klemp and Wilhelmson, 1978). If none of these features were present, the thunderstorm was classified as a single-cell thunderstorm.

In addition, some cases had Doppler radar data that was not sufficient enough to confidently classify the thunderstorm, so sounding data from the nearest upper-air station were used to aid in the classification. On these soundings shear was analyzed. Based on Weisman and Klemp (1982), a single-cell thunderstorm was selected when shear values were less than 10 m/s; multicellular thunderstorms were selected in sheared environments between 5 and 15 m/s; and lastly supercell thunderstorms were selected in environments with shear greater than 20 m/s. It is important to note that not every case followed the theory outlined by Weisman and Klemp (1982), but for many cases it did apply. In cases where the Doppler radar data and sounding data from the University of Wyoming upper air sounding archive (University of Wyoming Department of Atmospheric Science, n.d.) did not allow for a high confidence subjective assessment, the wind data was omitted from the analysis. In total, 8.7% of the cases were removed. Fig. 7 depicts the general methodology discussed above for classifying thunderstorm events by thunderstorm type through the utilization of the reflectivity and velocity radar data on the left, and if needed, the 0–6 km shear data on the right. Examples of the classification are shown in the next section.

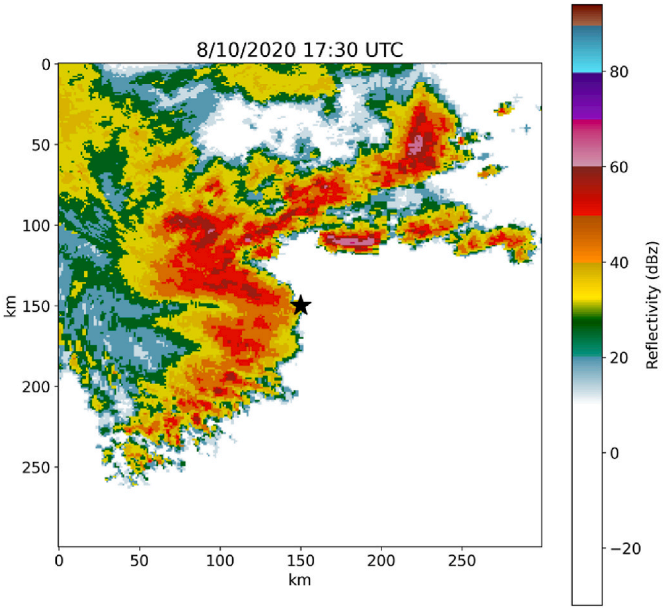

Fig. 6. 186 miles by 186 miles (300 km by 300 km) reflectivity mosaic centered on KCID showing the August 10, 2020 derecho in Iowa. The case fits the description of a multicellular thunderstorm type.

2.3. *Classification examples*

A thunderstorm event on August 10, 2016 was classified as a single-cell thunderstorm and had a raw (recorded) wind speed of 53 kt (61 mph or 27 m/s). In the Doppler radar data, the cell is isolated and only lasts for approximately 1 h. The isolated nature of the cell can be seen in the reflectivity plot of Fig. 8 where a small circular region is near the station denoted by the star. While other areas of high reflectivity exist, they are not connected by regions of lighter precipitation. There is likely not a hail core present as the reflectivity is below 60 dBZ (Lemon, 1998), and the velocity does not show any rotation in the thunderstorm. This rules out the possibility of a supercell thunderstorm, meaning the likely thunderstorm type is single-cell.

On July 19, 2018, the thunderstorm type was classified as a supercell due to the original cell splitting and the velocity image showing rotation in the thunderstorm. An area of rotation is apparent in Fig. 9 where high values of velocity, indicated by red (away) and green (towards) the radar, are seen on velocity plots adjacent to each other. In addition, a hook echo can be identified in the reflectivity data of Fig. 9 evident by the downward extrusion of high reflectivity values on the southwest side of the thunderstorm. Iowa had 28 tornado reports on this day, including one associated with this supercell thunderstorm near Pella, IA which is approximately 13 miles (21 km) northwest of the ASOS station (NOAA, 2018). A wind speed of 62 kt (71 mph or 32 m/s) was recorded for this supercell thunderstorm event.

A multicellular thunderstorm occurred on August 27, 2004 and produced winds of 54 kt (62 mph or 28 m/s). Fig. 10 depicts a thunderstorm with a large spatial extent of convective precipitation. This precipitation is organized in a linear line and is bowing outward, as the thunderstorm approaches the station. This line of convective precipitation appears to meet the criteria of an MCS (Houze, 1993).

In some cases, Doppler radar data analysis alone was not sufficient to identify the thunderstorm type. In the Doppler radar data from June 18, 2014, an isolated cell with rotation appears to be associated with the 57 kt (66 mph or 29 m/s) recorded wind speed in Fig. 11. However, bands of missing data in the reflectivity and velocity plots due to the distance from the radar make it hard to determine the isolated nature of the thunderstorm. For this reason, a sounding and mosaic plot was also used with the Doppler radar data. The sounding in Fig. 12 confirms the presence of enough 0–6 km wind shear present in the environment to support a supercell. This is seen by the wind barbs on the y-axis which change in both direction and magnitude between 1000 mb and 700 mb. The 0–6 km shear value is approximately 17 m/s which falls between the multicellular and supercell thunderstorm values (Weisman and Klemp, 1982). The reflectivity mosaic data along with the tornado warning issued for this thunderstorm confirmed the suspected supercell classification indicated by the 0–6 km shear values.

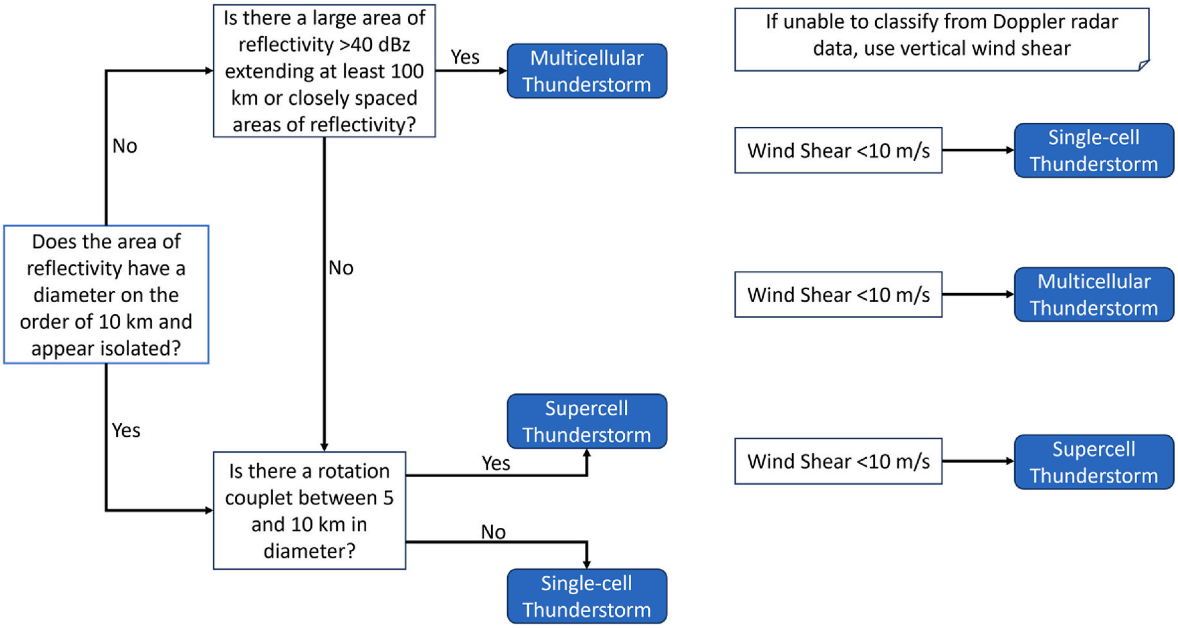

Fig. 7. Flowchart giving an overview of the methods section used for classifying thunderstorm events from Doppler radar data. The decision tree is general guidance and may not work for all cases.

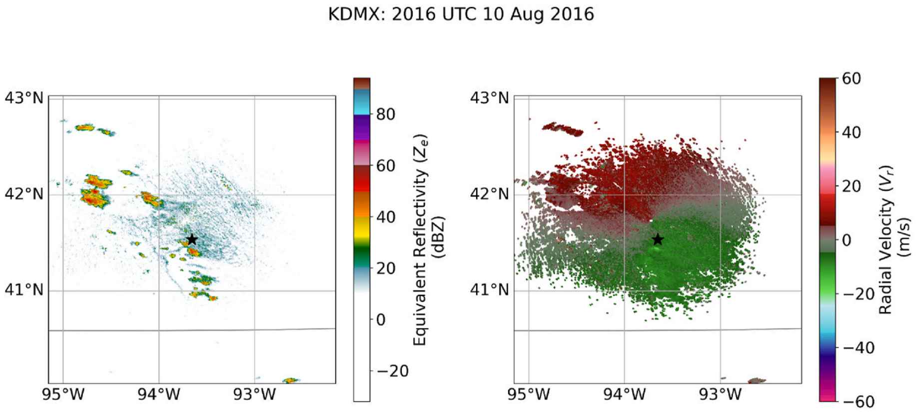

Fig. 8. The left image is the reflectivity plot, and the right image is the velocity plot for August 10, 2016 at the lowest elevation scan of the radar. The black star in the center is the location of the ASOS station.

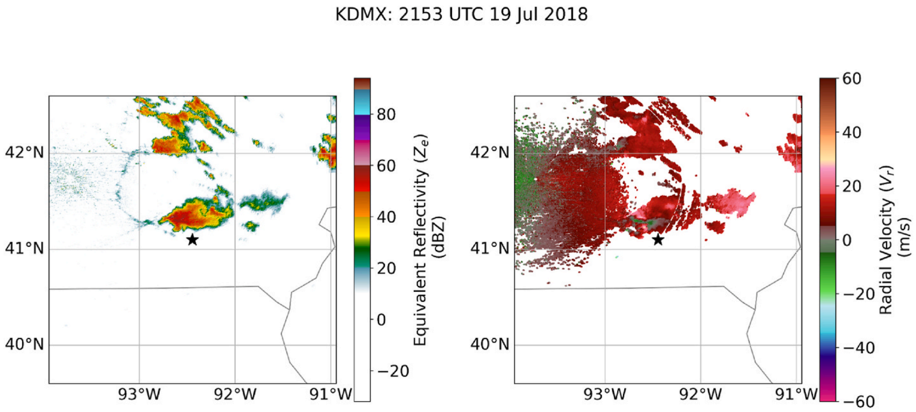

Fig. 9. The left image is the reflectivity plot, and the right image is the velocity plot for July 19, 2018 at the lowest elevation scan of the radar. The velocity plot has a rotation couplet in the same area of the hook, indicating a supercell thunderstorm.

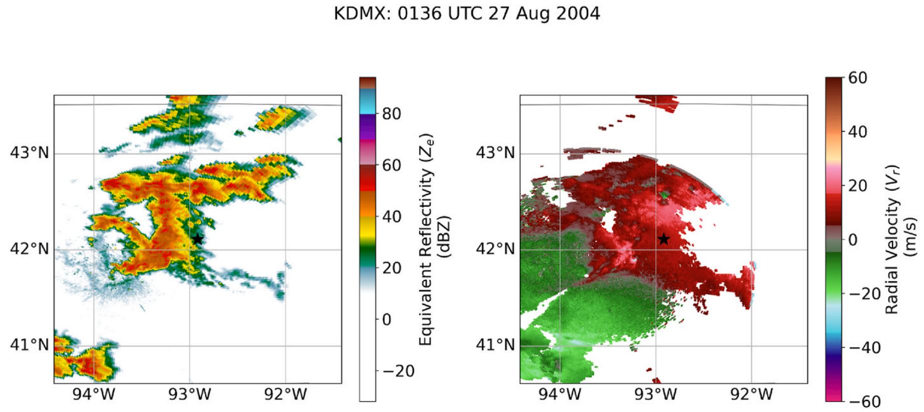

Fig. 10. The left image is the reflectivity plot, and the right image is the velocity plot for August 27, 2004 at the lowest elevation scan of the radar.

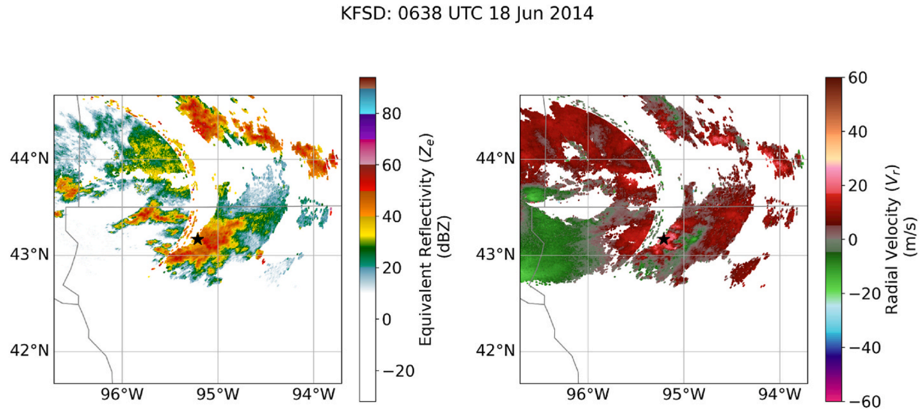

Fig. 11. The left image is the reflectivity plot, and the right image is the velocity plot for June 18, 2014 at the lowest elevation scan of the radar. Based on the Doppler radar data alone, it is hard to tell if the thunderstorms were discrete and if rotation is present due to missing data in the region of the ASOS station.

2.4. Analysis and results

Between the years of 1996 and 2022 (excluding 2001), 359 events were flagged as independent thunderstorm events above 50 kt (58 mph or 26 m/s) which included all 15 ASOS stations. To ensure statistical independence for each data point across space, only the highest wind speed within a 3-h time period was kept for multicellular thunderstorms. As for supercells and single-cell thunderstorms, any events that occurred within 3 h of each other were compared to ensure the thunderstorms were different. This resulted in 234 independent non-synoptic events in Iowa. Of these 234 events, 19 events had a low confidence rating for the thunderstorm type, so these were omitted from the analysis. Fig. 13 shows the breakdown of the remaining wind events by month and by year. Around 2008, an increase in the number of events per year greater than 50 kt (58 mph or 26 m/s) can be seen in Fig. 13b. This is likely due to the change from cup anemometers to sonic anemometers (Lombardo, 2012). Additionally, Fig. 13c shows a peak in the number of high wind events in June which is when the environment is most favorable for thunderstorms to develop in Iowa.

Fig. 13a shows the distribution of the events based on the thunderstorm type. In Iowa, 80% of the cases are multicellular thunderstorms. Of these multicellular thunderstorms, 80% are mesoscale convective systems specifically. Single-cell thunderstorms amount to approximately 14% and supercells amount to 6% of the cases, respectively. The high number of multicellular thunderstorm events is most likely due to the thunderstorm type being one of the most common thunderstorm modes, but also due to the large spatial coverage of this thunderstorm type. In Iowa, it is common to see upscale growth of single-cell and supercell thunderstorms, where the individual thunderstorms congeal into an organized line (Markowski and Richardson, 2010). The area that these multicellular thunderstorms impact is significantly higher than the area a supercell or single-cell thunderstorm would cover. ASOS stations are a single point in space, so it is easier to capture an event with any one ASOS station spanning a whole state versus an individual thunderstorm that only spans 10 km (6.2 mi).

2.5. Extreme value analysis

2.5.1. Data and methods

After the classification of all events by thunderstorm type, an extreme-value analysis was completed. A ‘superstation’ type approach was used where all the data points from Iowa were combined into one large station (Peterka and Shahid, 1998) over the defined time period. The events were already checked for independence during the classification. Table 2 shows the average rate of independent thunderstorm events above 50 kt (58 mph or 26 m/s) for the state of Iowa between 1996 and 2022. Once the data had been grouped, an extreme-value analysis was employed for the 3-s 10 m gust speed by fitting a Gumbel distribution (Simiu and Heckert, 1996). The standardization process for the ASOS data is discussed in Lombardo (2012). The scale and location parameters were estimated by using the method of moments (Hosking et al., 1985). Fitting the Gumbel distribution and the subsequent extrapolation is common practice in engineering for any storm type (e.g., Walshaw, 1994; Holmes, 2015; Bakker et al., 2021; Lombardo and Zickar, 2020). A Gumbel-like distribution was used for all wind speeds in ASCE 7 wind maps (American Society of Civil Engineers, 2022; Pintar et al., 2015) and so the Gumbel fit here provides a similar methodology to make comparisons.

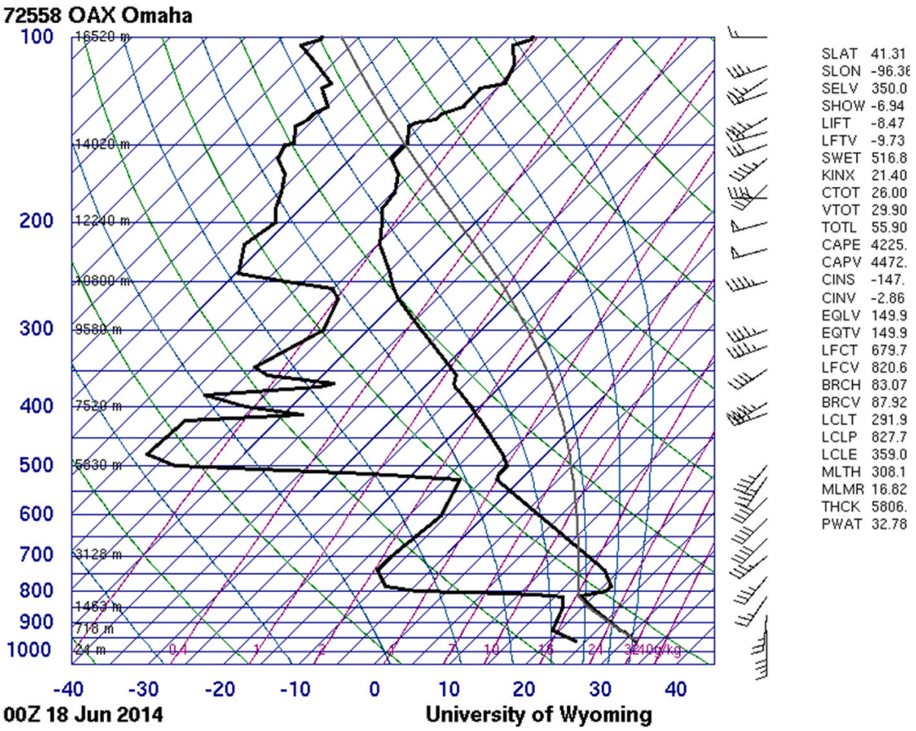

Fig. 12. The sounding from Omaha, Nebraska, taken near the thunderstorm on June 18, 2014. On the left y-axis is the pressure level in millibars and to the right in smaller text is the corresponding height in meters. The wind barbs on the right y-axis represent the wind speed and direction at the corresponding pressure level in knots. Plot from University of Wyoming Department of Atmospheric Science (n.d.).

2.5.2. Results

Fig. 14 shows the return period versus 3-s 10 m gust speed relationships for each thunderstorm type along with all the non-synoptic events grouped together. The return periods of 300, 700, 1700 and 3000 years are plotted as these correspond to ASCE risk categories (American Society of Civil Engineers, 2022). Fig. 14 shows for all non-synoptic events and multicellular thunderstorms, the wind speed associated with a 10-year return period is approximately 87 mph (39 m/s) and 86 mph (38 m/s) respectively. Whereas for single-cell and supercell thunderstorms the 10-year wind is 76 mph (34 m/s) and 70 mph (31 m/s) respectively. Supercell thunderstorms have the lowest wind speeds with the associated return periods of ASCE 7–22 (American Society of Civil Engineers, 2022). Multicellular thunderstorms and all non-synoptic events, have almost identical return periods for the same wind speed, and have higher wind speeds than single-cell thunderstorms and supercell thunderstorms, suggesting dominance of the multicellular thunderstorm type. For the 1700-year return period, multicellular thunderstorms have an estimated wind speed of 116 mph (52 m/s) and non-synoptic events as a whole, 117 mph (52 m/s). Table 3 depicts the wind speeds for each thunderstorm type and return period defined by ASCE 7–22 (American Society of Civil Engineers, 2022). Specifically, MCSs are the main thunderstorm type that causes these extreme winds. What is unknown is how these multicellular thunderstorms (along with supercell thunderstorms and single-cell thunderstorms) impact the loading on structures due to their characteristics (e.g., wind properties).

3. Wind speed estimation

As stated earlier, although ASOS stations can provide data for extreme value analysis, for the August 10, 2020 derecho, one of the stations (KCID) from the most heavily damaged area, Cedar Rapids, lost power during the time of most intense winds. This occurrence is common in extreme windstorms (Powell, 1993). Given the amount of damage in the Cedar Rapids area and the apparent significance of the event, the authors traveled to the area to perform a post-storm damage assessment. The objectives of the assessment were to perform (1) an estimation of wind speed through all methods including damage and to assess (2) the performance of urban and suburban infrastructure with focus on heavily damaged buildings. The focus of this section will be the results of the first objective. The areas surveyed include a 'northern' site near the Marion, IA area (i.e., Royal Oak Ridge) and a 'southern' site in SW Cedar Rapids which surrounded Wiley Plaza apartment complex, which was heavily damaged. These locations are shown in Fig. 15. Given the large spatial scale of this event, it was assumed that the magnitude of peak wind speed in areas surveyed around Cedar Rapids was approximately the same.

The first task of the wind speed estimation was bounding the range of possible peak wind speeds using damage to traffic signs. Traffic signs have been used in a number of publications (e.g., Rhee et al., 2022) to arrive at possible lower bound wind speeds (failed signs) and upper bound wind speeds (unfailed signs). The wind speed estimation process is described in detail in Rhee et al. (2022) but is described briefly here. For each sign (failed or unfailed), the sign and supporting pole dimensions are measured. These dimensions include the surface area of the sign (or signs), height of the sign centroid above ground level and cross-sectional properties of the supporting pole. If available, samples of the supporting poles were acquired and tested in the structures laboratory at the University of Illinois using three-point bending tests to calculate the point load required to fail the sample. This load is then used to calculate a bending moment required to produce failure (M_f) (Eq. (1)) If a sample was not able to be obtained, the geometric properties of the sign post (e.g., elastic modulus) as well as its yield stress were obtained and used to calculate M_f. The M_f value is then coupled with the sign aerodynamics (i.e., drag coefficient) to estimate a failure wind speed, V_c, for each sign (Eq. (2)). It should be noted that the moment diagram from three-point bending test is different from that of a cantilevered sign, which was the condition in the field.

A total of 14 signs (10 from southern site and 4 from northern site) were collected and measured. General exposure conditions were 'open' for the northern location (Royal Oak) and 'suburban' for the southern

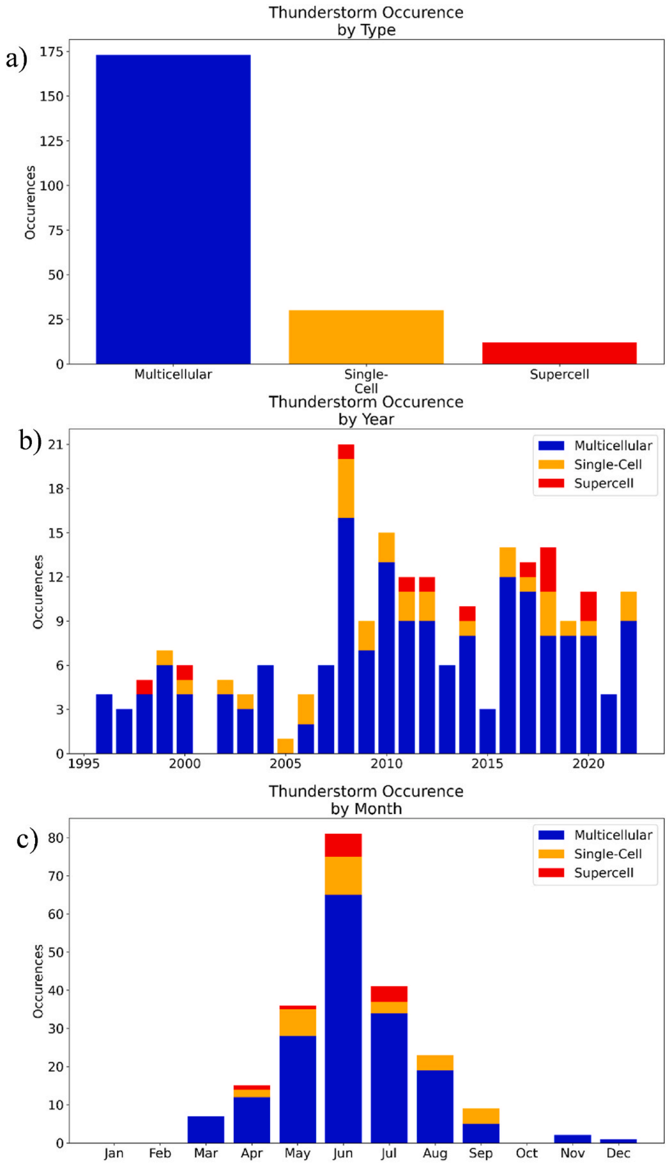

Fig. 13. Thunderstorm type classification for events in Iowa from 1996 to 2022. Top: By thunderstorm type; middle: By year and thunderstorm type; and bottom: By month and thunderstorm type.

Table 2
The total number and annual mean of independent thunderstorm events with a wind speed greater than 50 kt (58 mph or 26 m/s) between the year 1996 and 2022 by thunderstorm type.

Thunderstorm Type	Number of Events	Annual Rate
Single-Cell Thunderstorm	31	1.2
Supercell Thunderstorm	12	0.5
Multicellular Thunderstorm	172	6.9
Non-Synoptic (All)	215	8.6

location (Wiley Plaza) given the approximate wind direction (Fig. 16). Based on wind directions and direction of fallen crops, wind direction at the time of the peak wind speed was assumed to be roughly perpendicular to the orientation of the traffic signs surveyed. Letchford (2001) found drag coefficients to be near constant ± 45 deg from perpendicular to the sign plate and estimated wind directions are believed to be well within this range.

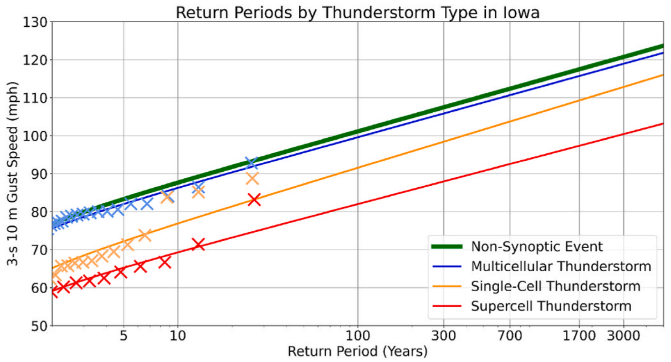

Fig. 14. The associated standardized 3-s 10 m gust speeds based on the return period. The solid lines are the estimated wind speeds and return periods for each thunderstorm type. The Xs are the individual events captured by the ASOS stations. This graph is valid for the state of Iowa from 1996 to 2022.

Table 3
The 3-s 10 m gust speed of different thunderstorm types for Iowa and the associated return periods. The ASCE 7–22 values are the combined synoptic and non-synoptic speed for Des Moines, IA. Values are shown in mph.

Thunderstorm Type	300-year	700-year	1700-year	3000-year
Single-Cell	98 mph	103 mph	109 mph	112 mph
Supercell	88 mph	93 mph	97 mph	100 mph
Multicellular	106 mph	111 mph	116 mph	119 mph
Non-synoptic (All)	107 mph	112 mph	117 mph	121 mph
ASCE 7–22	103 mph	110 mph	117 mph	122 mph

$$M_f = \frac{PL}{4} \tag{1}$$

$$V_c = \sqrt{\frac{M_f}{0.5\rho A z C_d}} \tag{2}$$

Where M_f is the bending moment at which the sign fails, P = is the failure load for the three-point bending tests (if applicable), L = length of sample (32 inches or 0.82 m from the UIUC testing), ρ = air density, A = surface area of the sign, z = is centroid height of the sign (or signs) and C_d = is the drag coefficient of the signs. The C_d values are based on aspect and clearance ratios in ASCE 7–22 (American Society of Civil Engineers, 2022), F igure 29.3–1. Fig. 17 shows an example of the process in the Marion area (northern area shown in Fig. 15).

Based on the sign analysis, a plot can be generated that illustrates the relationship between V_c and z is shown in Fig. 18. The V_c values greater than 140 mph (63 m/s) are left off of this plot and were all upper bound values (i.e., unfailed signs). In Fig. 18 there appears to be a break in V_c where signs with V_c below a certain value mostly failed and the signs above that value remained standing with the ‘failing’ sign near the boundary of the break. The ‘failing’ sign is therefore thought to be important to the wind speed estimation and can be used in the wind speed estimation process as either a highest lower bound (i.e., sign failure) or lowest upper bound (i.e., sign non-failure). A line is added in Fig. 18 denoting this use of this bound as the lowest upper bound. Based on the assessment the sign had permanent deformation at the base of the post, however it had not been completely driven to the ground as shown in the first two sign images in Fig. 17. The lowest upper bound value (sign failure) is also denoted in Fig. 18 as 79 mph (35 m/s) and so estimated wind speeds were thought to fall between these values at their respective heights.

In addition to the wind speed range and based on the damage survey, exposure was also thought to be a significant factor in the levels of damage including from signs. Given these observations, two profiles were added in Fig. 18. Fig. 18 shows profiles for z0 = 0.2 m (0.66 ft), a

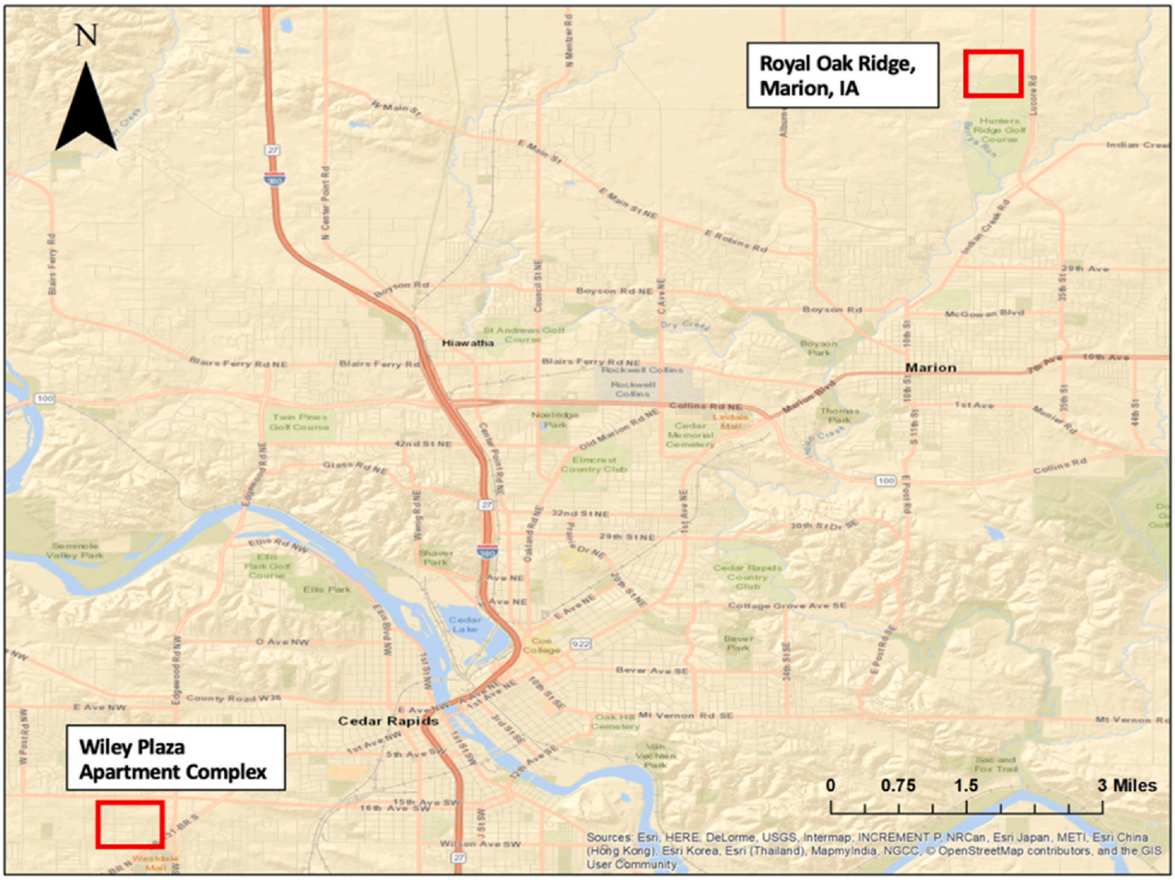

Fig. 15. Map showing the damage survey locations in the Cedar Rapids, IA vicinity denoted by red boxes.

roughness length more indicative of suburban terrain and the southern area surveyed and $z0 = 0.03$ m (0.1 ft), more indicative of the northern site and 'open' terrain. Given the known long duration of the event from reports and the wide spatial expanse of extreme winds in this derecho, the profile shape was assumed to follow the log law close to the surface and for the entire Cedar Rapids area. Given this assumption the profiles in Fig. 18 correspond to a 3-s averaging time (U_3) and was developed based on Masters et al. (2010). The open terrain profile was made to approximately fit through the 'failing' z and V_c pair (9 ft, 94 mph or 2.7 m, 42 m/s). The same process was carried out with the suburban terrain profile. The x-axis also includes the label 'U_3', which indicates the assumption $V_c = U_3$ and discussion will be in terms of wind speed from this point on.

As an example of the significance of exposure, the gust wind speed for open terrain at 20 ft (6.1 m) is approximately 108 mph (48 m/s) while $z0 = 0.2$ m (0.66 ft) at 10 ft (3.05 m) is approximately 76 mph (33 m/s). These ranges of height and exposure are roughly the ranges observed for the structures surveyed in the Cedar Rapids area. The profiles shown in Fig. 19 also give some measure of uncertainty in wind speed estimation based on the assumption of terrain condition and height above ground. For example, also added in Fig. 18 is a dotted line which represents the highest lower bound from the suburban terrain at 90 mph (40 m/s) (Sign #2). This wind speed at the height of failure is near the bound of the open terrain profile. Based on the estimation procedure the log profile gives a 10 m, 3-s gust of approximately 118 mph (53 m/s) in open terrain. The implications of this estimation will be discussed in the following paragraphs.

A note on the estimation process from signs and its limitations in addition to the relatively small sample size. The coefficient of variation in M_f from the bending tests was approximately 3%. When this 3% is applied to M_f in the calculation of V_c this amounts to an approximately 3% difference in the critical wind speed, V_c. As another example, a wind gust with an averaging time less than 3-s may be responsible for sign failure. Any averaging time and terrain condition can be used in this method and a log law profile need not be assumed. In addition, the analysis assumed no dynamic effects of the sign, eccentricities in loading or considered drag coefficient as a function of angle attack. A more rigorous wind speed estimation method could try to include these factors and optimize the log law fit to the observed data by varying the parameters used in estimation. Fragility curves could be developed based off the proportion of sign failures and V_c and a Monte Carlo simulation procedure could be carried out.

The second task for wind speed estimation was to investigate anemometers in the nearby vicinity of Cedar Rapids based on the preliminary reports of extreme wind speeds measured. The ASOS station, KCID (Cedar Rapids), was confirmed to have lost power at approximately 12:30 p.m. local time. KCID recorded a 3-s peak wind gust of 68 mph (30 m/s) (NOAA, 2020c) before losing power. The damage in the area was suggestive of much higher wind speeds. The first anemometer investigated was in nearby Atkins, approximately 7.5 miles (12 km) west-northwest of Cedar Rapids. This anemometer was reported to have produced a 126 mph (56 m/s) gust. This report was archived by the National Weather Service (NWS) and appears in post-storm assessment documentation (NOAA, 2020c). This report was relayed to the survey team by the NWS before leaving to perform the damage assessment. The team traveled to its location and talked with the owner of the anemometer, which was sited above their home at approximately 25 feet (7.6 m) above the ground based on drone imagery. Upon talking to the owner, it was learned that no data was archived and the report was relayed to a neighbor who then called the NWS. Given the anemometer siting (prone to speed ups) and type (cup anemometer) and the minimal observed damage inconsistent with the measured wind speed at and

Fig. 16. Aerial images where sign damage was surveyed. The red boxes indicate the locations where the signs were located. *Top:* Northern survey area with image from the authors; *Bottom:* Southern survey area with image from Google Earth. Approximate wind direction is shown with white arrow in both images.

around the site it was determined that this report was likely not reliable. This measurement will still be shown for the analysis in the following paragraphs.

An additional search of nearby anemometers was carried out following the post-storm survey. A total of three additional records were found and utilized in this study. Sources included the Marshalltown, IA, ASOS station (KMIW) at approximately 65 miles (105 km) west of KCID, an anemometer maintained by the cooperative weather observer program (CWOP) from Marion, IA, (data provided by WeatherFlow) which was approximately 1.5 miles (2.4 km) from the observed sign damage in the northern survey area, and a third nearby anemometer in North Liberty, IA, approximately 12 miles (19.3 km) from KCID maintained by the local emergency management agency and recorded a full time history of the event (Henson, 2021). Height and averaging time for the KMIW ASOS are standard. Estimated heights were provided for the CWOP station (between 10 and 12 ft) and the N. Liberty EMA (15 ft), however the averaging time and terrain conditions for these gust wind speed data are unknown. Fig. 19 shows the wind speeds for these

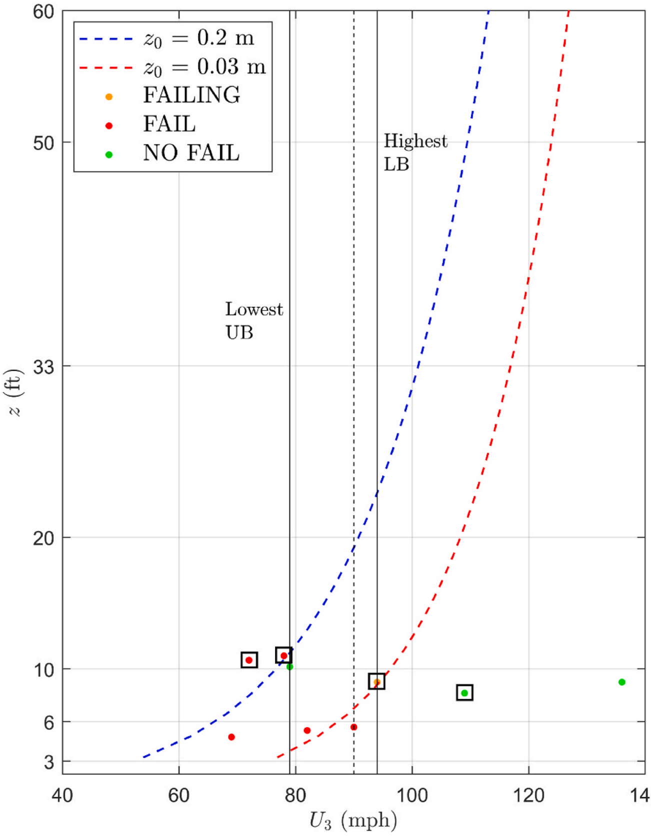

Fig. 18. Relationship between V_c and z of the surveyed signs in the Cedar Rapids area including the log law profiles for two terrains. Squares denote signs that were surveyed in open terrain (northern site). Dotted vertical line represents the highest lower bound (failed sign) value from the southern site (suburban terrain).

Fig. 17. Example of failed and unfailed signs from the August 10, 2020 derecho. These images show signs in the Marion area (northern site).

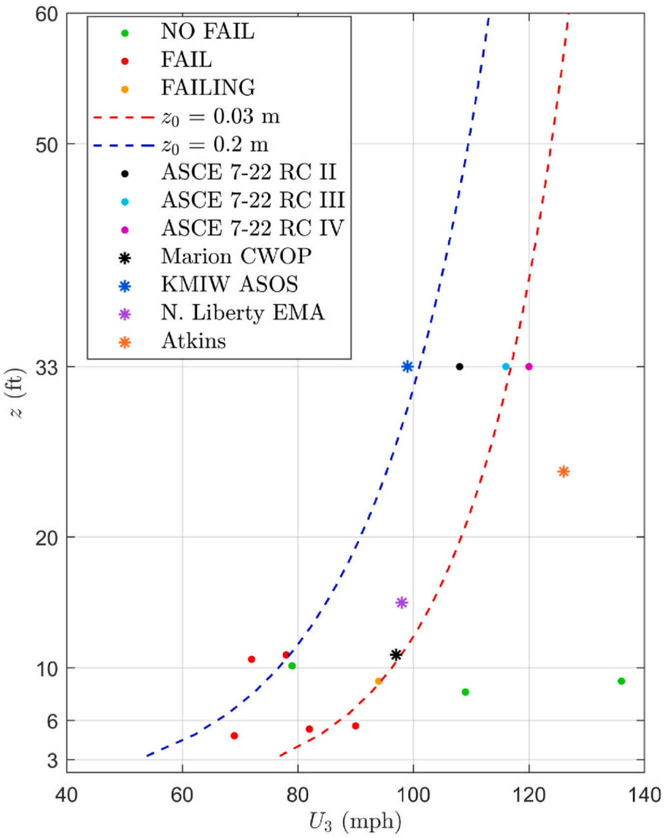

Fig. 19. Plot showing the wind speed values obtained from various sources overlaid with both log law profiles and ASCE basic wind speed values.

locations in addition to estimates derived previously. The peak gust at KMIW was 99 mph (44 m/s) (NOAA, 2020c), however this value is not in the archived data. The reason for lack of archival is that the primary power was also lost at this station; however, employees at the National Weather Service (NWS) in Des Moines called the automated line where the 99 mph (44 m/s) value was relayed via recording (NWS, personal communication). This value is likely not the true peak wind speed for this event in that location. The CWOP value located near the sign damage in Marion is very close to the log law estimation based on the sign damage, though the observer reported the mast was toppled in the derecho so wind speeds could have been higher. The other two data points are close to the bounds provided by the log law fits for the two terrain conditions. The Atkins measurement falls well outside the expected bounds of the profiles.

Also included in Fig. 19 are the ASCE 7–22 (American Society of Civil Engineers, 2022) ‘basic’ (non-tornado) wind speed values for Risk Categories II through IV. These values are representative of a 3-s gust in open terrain, similar to the log profile for z0 = 0.03 m. The estimated 10 m, 3-s gust of approximately 118 mph (53 m/s) in open terrain, corresponds to a roughly 1700-year mean recurrence interval (MRI) in ASCE 7. The extreme value analysis illustrated in Fig. 14 also shows similar wind speed values for both multicellular thunderstorms and all non-synoptic events together.

Fig. 20 shows the associated return periods when the 118 mph (53 m/s) wind speed estimate is added to the dataset for the extreme value analysis conducted and discussed previously. The 118 mph (53 m/s) value causes a higher wind speed estimation for both multicellular thunderstorms and the combined non-synoptic curve, as expected. The addition of this data point changes an event with a similar magnitude as the August 10, 2020 derecho from an approximate 1700-year event to a 700-year event. This finding shows that one extreme event can impact the extreme value analysis greatly.

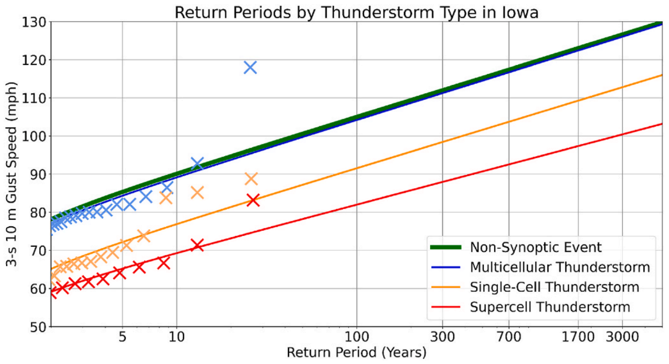

Fig. 20. The associated standardized 3-s 10 m gust speeds based on the return period. The derecho event is a 1 in 700-year event when the 118 mph (53 m/s) wind speed is included in the data. The solid lines are the estimated wind speeds and return periods for each thunderstorm type. The Xs are the individual events captured by the ASOS stations. This graph is valid for the state of Iowa from 1996 to 2022.

4. Conclusions and future work

The August 10, 2020 derecho that impacted Iowa and other nearby states is the costliest thunderstorm disaster in U.S. history as of 2023. Based on local accounts and limited field data, this event was unique in that extreme winds capable of causing significant damage persisted for a relatively long period of time. This event prompted the asking of two research questions: (1) should derechos, and their broader thunderstorm type, multicellular thunderstorms, be considered separately when predicting extreme wind speeds for wind load design? and (2) how unique is this particular event in the context of wind engineering?

The current extreme value analysis used for building design does not directly consider thunderstorm type and instead uses a binary and mixed-distribution approach of synoptic and non-synoptic winds. Breaking events up into synoptic and non-synoptic might not be sufficient as each thunderstorm type has different physical (e.g., spatial and temporal) and probabilistic characteristics. Through a classification procedure that included analysis of Doppler radar data and environmental conditions, this paper separates thunderstorm winds into three types: single-cell thunderstorms, multicellular thunderstorms, and supercell thunderstorms.

A dataset was created using Iowa ASOS data of thunderstorm wind events above 50 kt (58 mph or 26 m/s). Doppler radar data were then created for each of the events, and the thunderstorm type was determined. In cases where Doppler radar analysis alone was not sufficient, soundings were used to estimate the environmental shear for the thunderstorm. The majority of the events between 1996 and 2022 were multicellular thunderstorms. The extreme-value analysis performed shows that multicellular thunderstorms, specifically mesoscale convective systems, dominate the climatology as wind speeds at given return periods for all non-synoptic events are similar to multicellular thunderstorms only.

However, we emphasize the need for additional, future studies to capture wind data from supercell and single-cell thunderstorm events within Iowa and elsewhere. As of this study, surface observations in Iowa consisted of only 15 ASOS stations. In this case, the excess of multicellular thunderstorms as compared to single-cell and supercell thunderstorms are likely due, at least in part, to the overall frequency and spatial resolution of such thunderstorms. The relatively small spatial scales associated with single-cell and supercell thunderstorms makes it difficult for the ASOS network to adequately sample these thunderstorm types with any regularity. In addition, as the wind speed increases, the likelihood of capturing an extreme wind event is significantly less with a sparse network compared to a dense network (Lombardo and Zickar, 2020). Future studies could utilize similar methodologies to those employed herein to compare stations in the ASOS network to denser networks such as the Oklahoma Mesonet to see if differences in the extreme values exist (e.g., Lombardo and Zickar, 2020), and to attempt to capture events more adequately with smaller spatial scales including single-cell and supercell thunderstorms.

For these reasons, ASOS stations may not be an accurate representation of the wind speed climatology in Iowa and the rest of the United States. In the Cedar Rapids area, severely affected by the August 10, 2020 derecho, the lone ASOS station lost power before the peak wind speed was reached. This power loss necessitated a wind speed estimation procedure which included sign damage and through a search of available wind data in the area. The estimated peak wind speed was approximately 118 mph (53 m/s) at standard height and terrain. This 118 mph (53 m/s) estimate, when added to the extreme value analysis, makes an event of this magnitude significantly more likely than would currently be expected.

In order to make the thunderstorm type classification process easier, a method that utilizes machine learning to classify thunderstorm mode is currently being developed. This will allow for the classification and the extreme value analysis methods described in this paper to be utilized for the entire United States. By doing so, the hope is to determine which thunderstorm type needs to be considered in specific regions of the United States and to encourage more focus and research on the characteristics of the surface winds and associated wind loading based on thunderstorm type.

CRediT authorship contribution statement

David T. Roegner: Writing – review & editing, Writing – original draft, Visualization, Validation, Software, Methodology, Investigation, Formal analysis, Data curation, Conceptualization. **Franklin T. Lombardo:** Writing – review & editing, Writing – original draft, Visualization, Validation, Supervision, Software, Resources, Project administration, Methodology, Investigation, Funding acquisition, Formal analysis, Data curation, Conceptualization. **Zachary B. Wienhoff:** Writing – review & editing, Visualization, Supervision, Project administration, Methodology, Investigation, Conceptualization. **Daniel M. Rhee:** Writing – review & editing, Visualization, Validation, Methodology, Investigation, Formal analysis, Data curation. **Melissa A. Wagner:** Writing – review & editing. **Richard L. Wood:** Writing – review & editing.

Declaration of competing interest

The authors declare that they have no known competing financial interests or personal relationships that could have appeared to influence the work reported in this paper.

Data availability

Data will be made available on request.

Acknowledgements

Rich Kinney and Ray Wolf of NWS Quad Cities are acknowledged for providing details on the Cedar Rapids area damage survey including wind measurements at the Atkins location. Brian Rammelsberg is acknowledged for sharing information about his anemometer at the Atkins location that recorded the 126 mph (56 m/s) value and allowing the team to fly the drone near the property and inspect both the anemometer and the surrounding damage. Chad Hahn from NWS Des Moines is thanked for providing details about the 99 mph (44 m/s) wind reading at the KMIW ASOS station. Ryan Pape who managed the CWOP station in Marion for the anemometer height at that location and Dave Wilson for assistance with the North Liberty EMA wind data and anemometer height are acknowledged. Weatherflow and David Roueche are acknowledged for providing nearby wind data for surrounding surface-based stations including the Marion CWOP station.

Funding is gratefully acknowledged from the National Science Foundation (NSF) for both the survey and research portions of this work. This research was supported by StEER CMMI-1841667, NSF RAPID AGS-2054706, NSF CAREER CMMI-2144760, and NSF Disaster Resilience Research Grant CMMI-2242578.

References

American Society of Civil Engineers, 2022. Minimum Design Loads for Buildings and Other Structures.

Atkins, N.T., Bouchard, C.S., Pryzybylinski, R.W., Trapp, R.J., Schmocker, G., 2005. Damaging surface wind mechanisms within the 10 June 2003 Saint Louis bow echo during BAMEX. Mon. Weather Rev. 133 (8), 2275–2296. https://doi.org/10.1175/MWR2973.1.

Bakker, F.P., Koker, N.D., Viljoen, C., 2021. Preconditioning wind speeds for standardised structural design. Eng. Struct. 238 https://doi.org/10.1016/j.engstruct.2021.111856.

Brooks, H.E., Lee, J.W., Craven, J.P., 2003. The spatial distribution of severe thunderstorm and tornado environments from global reanalysis data. Atmos. Res. 67–68, 73–94. https://doi.org/10.1016/S0169-8095(03)00045-0.

Burgess, D.W., 1976. Single Doppler radar vortex recognition: Part I–Mesocyclone signatures. In: 17th Conference on Radar Meteorology, Seattle, pp. 97–103.

Byers, H.R., Braham Jr., R.R., 1948. The Thunderstorm. U.S. Department of Commerce, Weather Bureau, Washington D.C.

Carbone, R.E., 1983. A severe frontal rainband. Part II: tornado parent vortex circulation. J. Atmos. Sci. 40 (11), 2639–2654. https://doi.org/10.1175/1520-0469(1983)040.

Davies-Jones, R.P., 2006. Tornadogenesis in supercell storms: what we know and what we don’t know. In: Symposium on the Challenges of Severe Convective Storms. American Meteorological Society, Atlanta, GA. https://ams.confex.com/ams/pdfpapers/104563.pdf.

Doswell III., C.A., Brooks, H.E., Kay, M.P., 2005. Climatological estimates of daily local nontornadic severe thunderstorm probability for the United States. Weather Forecast. 20 (4), 577–595. https://doi.org/10.1175/WAF866.1.

Doswell III., C.A., 1985. The Operational Meteorology of Convective Weather. Volume II: Storm Scale Analysis. NOAA. Technical Memorandum ERL ESG-15.

Fujita, T.T., Wakimoto, R.M., 1981. Five scales of airflow associated with a series of downbursts on 16 july 1980. Mon. Weather Rev. 109 (7), 1438–1456. https://doi.org/10.1175/1520-0493(1981)109%3C1438:FSOAAW%3E2.0.CO;2.

Gunter, W.S., Schroeder, J.L., 2015. High-resolution full-scale measurements of thunderstorm outflow winds. J. Wind Eng. Ind. Aerod. 138, 13–26. https://doi.org/10.1016/j.jweia.2014.12.005.

Haberlie, A.M., Ashley, W.S., 2019. A radar-based climatology of mesoscale convective systems in the United States. J. Clim. 32 (5), 1591–1606. https://doi.org/10.1175/JCLI-D-18-0559.1.

Henson, Bob. “Fierce Winds, Tornado Threat Looming for Wisconsin.” *Yale Climate Connections*, 28 July 2021, yaleclimateconnections.org/2021/07/fierce-winds-tornado-threat-looming-for-wisconsin/.

Holmes, J.D., 2015. Wind Loading of Structures, third ed. CRC Press. https://doi.org/10.1201/b18029.

Hosking, J.R.M., Wallis, J.R., Wood, E.F., 1985. Estimation of the generalized extreme-value distribution by the method of probability-weighted moments. Technometrics 27 (3), 251–261. https://doi.org/10.1080/00401706.1985.10488049.

Houze, R.A., Rutledge, S.A., Biggerstaff, M.I., Smull, B.F., 1989. Interpretation of Doppler weather radar displays of midlatitude mesoscale convective systems. Bull. Am. Meteorol. Soc. 70 (6), 608–619. https://doi.org/10.1175/1520-0477(1989)070<0608:IODWRD>2.0.CO;2.

Houze, R.A., 1993. Cloud Dynamics. Academic Press.

Ibrahim, I., Kopp, G.A., Sills, D.M.L., 2023. Retrieval of peak thunderstorm wind velocities using WSR-88d weather radars. J. Atmos. Ocean. Technol. 40 (2), 237–251. https://doi.org/10.1175/JTECH-D-22-0028.1.

Johns, R.H., Hirt, W.D., 1987. Derechos: widespread convectively induced windstorms. Weather Forecast. 2 (1), 32–49. https://doi.org/10.1175/1520-0434(1987)002.

Kelly, D.L., Schaefer, J.T., Doswell III., C.A., 1985. Climatology of nontornadic severe thunderstorm events in the United States. Mon. Weather Rev. 113 (11), 1997–2014. https://doi.org/10.1175/1520-0493(1985)113.

Klemp, J.B., Rotunno, R., 1983. A study of the tornadic region within a supercell thunderstorm. J. Atmos. Sci. 40 (2), 359–377. https://doi.org/10.1175/1520-0469(1983)040.

Klemp, J.B., Wilhelmson, R.B., 1978. The simulation of three-dimensional convective storm dynamics. J. Atmos. Sci. 35, 1070–1096. https://doi.org/10.1175/1520-0469(1978)035<1070:TSOTDC>2.0.CO;2.

Lemon, L.R., 1998. The radar “three-body scatter spike”: an operational large-hail signature. Weather Forecast. 13 (2), 327–340. https://doi.org/10.1175/1520-0434(1998)013%3C0327:TRTBSS/3E2.0.CO;2.

Lemon, L.R., Doswell III., C.A., 1979. Severe thunderstorm evolution and mesocyclone structure as related to tornadogenesis. Mon. Weather Rev. 107 (9), 1184–1197. https://doi.org/10.1175/1520-0493(1979)107.

Letchford, C.W., 2001. Wind loads on rectangular signboards and hoardings. J. Wind Eng. Ind. Aerod. 89 (2), 135–151. https://doi.org/10.1016/S0167-6105(00)00068-4.

Lombardo, F.T., 2012. Improved extreme wind speed estimation for wind engineering applications. J. Wind Eng. Ind. Aerod. 104, 278–284. https://doi.org/10.1016/j.jweia.2012.02.025.

Lombardo, F.T., Main, J.A., Simiu, E., 2009. Automated extraction and classification of thunderstorm and non-thunderstorm wind data for extreme-value analysis. J. Wind Eng. Ind. Aerod. 97 (3–4), 120–131. https://doi.org/10.1016/j.jweia.2009.03.001.

Lombardo, F.T., Smith, D.A., Schroeder, J.L., Mehta, K.C., 2014. Thunderstorm characteristics of importance to wind engineering. J. Wind Eng. Ind. Aerod. 125, 121–132. https://doi.org/10.1016/j.jweia.2013.12.004.

Lombardo, F.T., Zickar, A.S., 2019. Characteristics of measured extreme thunderstorm near-surace wind gusts in the United States. J. Wind Eng. Ind. Aerod. 193 https://doi.org/10.1016/j.jweia.2019.103961.

Lombardo, F.T., Zickar, A.S., 2020. Prediction of non-synoptic wind speeds. In: Hangan, H., Kareem, A. (Eds.), The Oxford Handbook of Non-synoptic Wind Storms. Oxford University Press, pp. 498–529.

Markowski, P.M., Richardson, Y.P., 2010. Mesoscale Meteorology in Midlatitudes. Wiley-Blackwell. https://doi.org/10.1002/9780470682104.

Marshall, J.S., Langille, R.C., Palmer, W.K., 1947. Measurement of rainfall by radar. J. Atmos. Sci. 4 (6), 186–192. https://doi.org/10.1175/1520-0469(1947)004%3C0186:MORBR%3E2.0.CO;2.

Masters, F.J., Vickery, P.J., Bacon, P., Rappaport, E.N., 2010. Toward objective, standardized intensity estimates from surface wind speed observations. Bull. Am. Meteorol. Soc. 91 (12), 1665–1682.

National Oceanic and Atmospheric Administration. (n.d.). Warning Criteria. National Weather Service. Retrieved December 3, 2022, from https://www.weather.gov/car/Warning_Criteria.

NOAA National Severe Storms Laboratory. (n.d.). Thunderstorm Types. https://www.nssl.noaa.gov/education/svrwx101/thunderstorms/types/.

National Weather Service, 1998. Automated surface observing system: user's guide. March. https://www.weather.gov/media/asos/aum-toc.pdf. (Accessed 21 November 2022).

NOAA, 2018. July 19, 2018 storm reports. Found online at. https://www.spc.noaa.gov/climo/reports/180719_rpts.html.

NOAA, 2020a. Billion dollar weather and climate disasters. Found online at. https://www.ncdc.noaa.gov/billions/events. (Accessed 21 June 2023).

NOAA, 2020b. Midwest derecho – August 10, 2020. Found online at. https://www.weather.gov/dvn/summary_081020.

NOAA, 2020c. August 10, 2020 derecho. Found online at. https://www.weather.gov/dmx/2020derecho.

NOAA, 2022. PERiLS: propagation, evolution, and rotation in linear storms. Found online at. https://www.nssl.noaa.gov/projects/perils/. (Accessed 7 September 2023).

NPR, 2020. Iowa derecho this August was most costly thunderstorm event in modern U. S. History. Found online. https://www.npr.org/2020/10/18/925154035/iowa-derecho-this-august-was-most-costly-thunderstorm-event-in-modern-u-s-histor. (Accessed 21 June 2023).

Peterka, J.A., Shahid, S., 1998. Design gust wind speeds in the United States. J. of Structural Engineering-Asce 124 (2), 207–214. https://doi.org/10.1061/(asce)0733-9445(1998)124:2(207.

Pintar, A.L., Simiu, E., Lombardo, F.T., Levitan, M.L., 2015. Maps of Non-hurricane Non-tornadic Wind Speeds with Specified Mean Recurrence Intervals for the Contiguous United States Using a Two-Dimensional Poisson Process Extreme Value Model and Local Regression.

Powell, M.D., 1993. Wind measurement and archival under the automated surface observing system (ASOS): user concerns and opportunity for improvement. Bull. Am. Meteorol. Soc. 74 (4), 615–624.

Rhee, D.M., Nevill, J.B., Lombardo, F.T., 2022. Comparison of near-surface wind speed estimation techniques using different damage indicators from a damage survey of naplate, IL EF-3 tornado. Nat. Hazards Rev. 23 (1), 04021052.

Schenkman, A.D., Xue, M., 2016. Bow-echo mesovortices: a review. Atmos. Res. 170, 1–13. https://doi.org/10.1016/j.atmosres.2015.11.003.

Simiu, E., Heckert, N.A., 1996. Extreme wind distribution tails: a "peaks over threshold" approach. J. Struct. Eng. 122 (5) https://doi.org/10.1061/(ASCE)0733-9445(1996)122:5(539.

Solari, G., 2014. Emerging issues and new frameworks for wind loading on structures in mixed climates. Wind Struct. 19 (3), 295–320. https://doi.org/10.12989/was.2014.19.3.295.

Stout, G.E., Huff, F.A., 1953. Radar records Illinois tornadogenesis. Bull. Am. Meteorol. Soc. 34 (6), 281–284. http://www.jstor.org/stable/26242141.

Trapp, R.J., 2013. Mesoscale-Convective Processes in the Atmosphere. Cambridge University Press.

Trapp, R.J., Weisman, M.L., 2003. Low-level mesovortices within squall lines and bow echoes. Part II: their genesis and implications. Mon. Weather Rev. 131 (11), 2804–2823. https://doi.org/10.1175/1520-0493(2003)131.

University of Wyoming Department of Atmospheric Science. (n.d.). Upper Air Soundings. Retrieve on August 9, 2023 from https://weather.uwyo.edu/upperair/sounding.html.

Vallis, M.B., Loredo-Souza, A.M., Ferreira, V., Nascimento, E.D.L., 2019. Classification and identification of synoptic and non-synoptic extreme wind events from surface observations in South America. J. Wind Eng. Ind. Aerod. 193, 103963 https://doi.org/10.1016/j.jweia.2019.103963.

Wakimoto, R.M., Murphey, H.V., Nester, A., Jorgensen, D.P., Atkins, N.T., 2006. High winds generated by bow echoes. part i: overview of the Omaha bow echo 5 July 2003 storm during BAMEX. Mon. Weather Rev. 134 (10), 2793–2812. https://doi.org/10.1175/MWR3215.1.

Wakimoto, R., 2001. Convectively driven high wind events. In: Doswell III, C.A. (Ed.), Severe Convective Storms. American Meteorological Society.

Walshaw, D., 1994. Getting the most from your extreme wind data: a step by step guide. J. of research of the National Institute of Standards and Technology 99 (4), 399–411. https://doi.org/10.6028/jres.099.038.

Weisman, M.L., 1992. The role of convectively generated rear-inflow jets in the evolution of long-lived mesoconvective systems. J. Atmos. Sci. 49 (19), 1826–1847. https://doi.org/10.1175/1520-0469(1992)049.

Weisman, M.L., Klemp, J.B., 1982. The dependence of numerically simulated convective storms on vertical wind shear and buoyancy. Mon. Weather Rev. 110 (6), 504–520. https://doi.org/10.1175/1520-0493(1982)110.

Wexler, R., Swingle, D.M., 1947. Radar storm detection. Bull. Am. Meteorol. Soc. 28 (4), 159–167. https://doi.org/10.1175/1520-0477-28.4.159.